Journal of Physics G: Nuclear and
Particle Physics

LETTER

Acoustic scaling of anisotropic flow in shape-engineered events: implications for extraction of the specific shear viscosity of the quark gluon plasma

To cite this article: Roy A Lacey *et al* 2016 *J. Phys. G: Nucl. Part. Phys.* **43** 10LT01

Acoustic scaling of anisotropic flow in shape-engineered events: implications for extraction of the specific shear viscosity of the quark gluon plasma

Roy A. Lacey,[1,2,*] D. Reynolds,[1] A. Taranenko,[1] N. N. Ajitanand,[1] J. M. Alexander,[1] Fu-Hu Liu,[1,3] Yi Gu,[1] and A. Mwai[1]

[1]*Department of Chemistry, Stony Brook University, Stony Brook, NY, 11794-3400, USA*

[2]*Department of Physics and Astronomy, Stony Brook University, Stony Brook, NY, 11794-3800*

[3]*Institute of Theoretical Physics, Shanxi University, Taiyuan, Shanxi 030006, China*

(Dated: July 14, 2016)

It is shown that the acoustic scaling patterns of anisotropic flow for different event shapes at a fixed collision centrality (shape-engineered events), provide robust constraints for the event-by-event fluctuations in the initial-state density distribution from ultrarelativistic heavy ion collisions. The empirical scaling parameters also provide a dual-path method for extracting the specific shear viscosity $(\eta/s)_{\rm QGP}$ of the quark-gluon plasma (QGP) produced in these collisions. A calibration of these scaling parameters via detailed viscous hydrodynamical model calculations, gives $(\eta/s)_{\rm QGP}$ estimates for the plasma produced in collisions of Au+Au ($\sqrt{s_{NN}} = 0.2$ TeV) and Pb+Pb ($\sqrt{s_{NN}} = 2.76$ TeV). The estimates are insensitive to the initial-state geometry models considered.

PACS numbers: 25.75.-q, 12.38.Mh, 25.75.Ld, 24.10.Nz

Considerable attention has been given to the study of anisotropic flow measurements in heavy-ion collisions at both the Relativistic Heavy Ion Collider (RHIC) and the Large Hadron Collider (LHC) [1–14]. Recently, the attack has focused on studies of initial state fluctuations and their role in the extraction of the specific shear viscosity (i.e. the ratio of shear viscosity to entropy density η/s) of the quark-gluon plasma (QGP) . These flow measurements are routinely quantified as a function of collision centrality (cent) and particle transverse momentum $p_{\rm T}$ by the Fourier coefficients v_n

$$v_n(p_{\rm T}, {\rm cent}) = \langle \cos[n(\phi - \Psi_{\rm n})] \rangle. \tag{1}$$

Here ϕ is the azimuthal angle of an emitted particle and $\Psi_{\rm n}$ is the estimated azimuth of the n-th order event plane [15, 16]; brackets denote averaging over particles and events. The current measurements for charged hadrons [17, 18] indicate significant odd and even v_n coefficients up to about the sixth harmonic.

The estimates of $(\eta/s)_{\rm QGP}$ from these v_n measurements have indicated a small value (i.e. 1-3 times the lower conjectured bound of $1/4\pi$ [19]). Substantial theoretical uncertainties have been assigned primarily to incomplete knowledge of the initial-state geometry and its associated event-by-event fluctuations. Indeed, an uncertainty of $\mathcal{O}(100\%)$ in the value of $(\eta/s)_{\rm QGP}$ extracted from v_2 measurements at RHIC ($\sqrt{s_{\rm NN}} = 0.2$ TeV) [5, 6], has been attributed to a $\sim 20\%$ uncertainty in the theoretical estimates [20, 21] for the event-averaged initial eccentricity ε_2 of the collision zone. Here, it is important to note that a robust method of extraction should not depend on the initial geometrical conditions since $(\eta/s)_{\rm QGP}$ is only a property of the medium itself.

Recent attempts to reduce the uncertainty for $(\eta/s)_{\rm QGP}$ have focused on: (i) the development of a more constrained description of the fluctuating initial-state geometry [22], (ii) the combined analysis of v_2 and v_3 [18, 23, 24] and other higher order harmonics [11] and (iii) a search for new constraints via "acoustic scaling" of v_n [25–27]. The latter two approaches [(ii) and (iii)] utilize the empirical observation that the strength of the dissipative effects which influence the magnitude of v_n(cent), grow exponentially as n^2 and $1/\bar{R}$ [25, 26, 28];

$$\frac{v_n({\rm cent})}{\varepsilon_n({\rm cent})} \propto \exp\left(-\beta\frac{n^2}{\bar{R}}\right), \;\; \beta \sim \frac{4}{3}\frac{\eta}{Ts}, \tag{2}$$

where ε_n is the n-th order eccentricity moment, T is the temperature and $\bar{R}$ is the initial-state transverse size of the collision zone. Thus, characteristic linear dependencies of $\ln(v_n/\varepsilon_n)$ on n^2 and $1/\bar{R}$ [cf. Eq. 2], are suggested with slopes $\beta' \sim \beta/R \propto (\eta/s)_{\rm QGP}$ and $\beta'' \sim n^2\beta \propto (\eta/s)_{\rm QGP}$.

These scaling patterns have indeed been validated and shown to point to important constraints for the extraction of $(\eta/s)_{\rm QGP}$ from data taken at both RHIC ($\sqrt{s_{\rm NN}} = 0.2$ TeV) and LHC ($\sqrt{s_{\rm NN}} = 2.76$ TeV) [25, 26]. Here, we explore new constraints for initial-state shape fluctuations, via scaling studies of v_n measurements obtained for shape-engineered events, i.e. different event shapes at a fixed centrality [29, 30].

Such constraints are derived from the expectation that the event-by-event fluctuations in anisotropic flow, result primarily from fluctuations in the size and shape (eccentricity) of the initial-state density distribution. Thus, various cuts on the full distribution of initial shapes [at a given centrality], should result in changes in the mag-

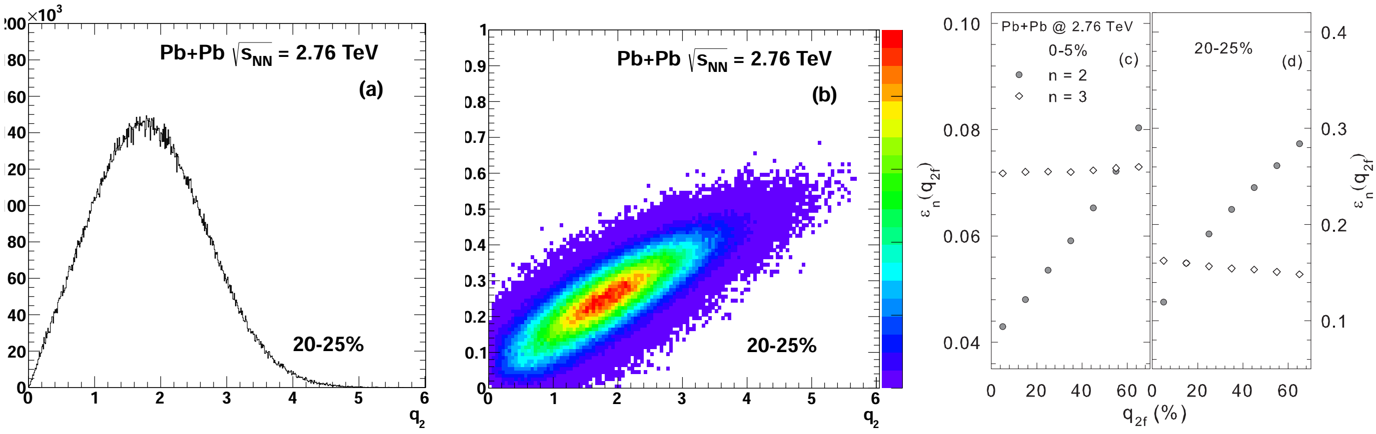

FIG. 1. (Color online) Calculated values for (a) the q_2 distribution for 20-25% central events; (b) ε_2 vs. q_2 for 20-25% central events; (c) $\varepsilon_{2,3}$ vs. $q_{2\mathrm{f}}$ for 0-5% central events; (d) $\varepsilon_{2,3}$ vs. $q_{2\mathrm{f}}$ for 20-25% central events. The calculations were made for Pb+Pb collisions at $\sqrt{s_{\mathrm{NN}}} = 2.76$ TeV with the MC-Glauber model.

nitudes of $\langle\varepsilon_n\rangle$, $\langle\bar{R}_n\rangle$ and $\langle v_n\rangle$. Note however, that acceptable models for the initial-state fluctuations should give $\langle\varepsilon_n\rangle$ and $\langle\bar{R}_n\rangle$ values each of which lead to acoustic scaling of $\langle v_n\rangle$ with little, if any, change in the slope parameter β' (β'') for different event shape selections, i.e., β' (β'') $\propto (\eta/s)_{\mathrm{QGP}}$ is a property of the medium, not the initial state geometry.

The q_n **flow vector** has been proposed [29] as a tool to select different initial shapes from the distribution of initial-state geometries at a fixed centrality;

$$Q_{n,x} = \sum_i^M \cos(n\phi_i);\ Q_{n,y} = \sum_i^M \sin(n\phi_i); \qquad (3)$$

$$q_n = Q_n/\sqrt{M}, \qquad (4)$$

where M is the particle multiplicity and ϕ_i are the azimuthal angles of the particles in the sub-event used to determine q_n. We use this technique for model-based evaluations of $\varepsilon_2(q_2,\mathrm{cent})$ and $\bar{R}(q_2,\mathrm{cent})$ to perform validation tests for acoustic scaling of recent $v_2(q_2,\mathrm{cent})$ measurements, as well as to determine if β'' is independent of event shape. Subsequently, we use the experimental acoustic scaling patterns in conjunction with the results of q_n-averaged viscous hydrodynamical calculations [31], to calibrate β' and β'' and make estimates of $(\eta/s)_{\mathrm{QGP}}$ for the plasma produced in Au+Au and Pb+Pb collisions at RHIC and the LHC respectively.

The data employed in this work are taken from measurements by the ALICE and CMS collaborations for Pb+Pb collisions at $\sqrt{s_{NN}} = 2.76$ TeV [30, 32], as well as measurements by the STAR collaboration for Au+Au collisions at $\sqrt{s_{NN}} = 200$ GeV [7, 33]. The ALICE measurements [30] exploit a three subevents technique to evaluate $v_2(q_2,\mathrm{cent})$, where the first subevent SE_1 is used to determine q_2, and the particles in the second subevent SE_2 are used to evaluate $v_2(q_2,\mathrm{cent})$ relative to the Ψ_2 event plane determined from the particles in the third subevent SE_3. To suppress non-flow correlations, the detector subsystems used to select $\mathrm{SE}_{1,2,3}$ were chosen so as to give a sizable pseudo-rapidity gap ($\Delta\eta_p$) between the particles in different subevents. For each centrality, $v_2(q_2)$ measurements were made for the full q_2 distribution [$v_2(q_{2(\mathrm{Avg.})})$], as well as for events with the 10% lowest [$v_2(q_{2(\mathrm{Lo})})$] and 5% highest [$v_2(q_{2(\mathrm{Hi})})$] values of the q_2 distribution.

The CMS [31] and STAR [33] $v_n(\mathrm{cent})$ measurements for $n = 2-6$ (CMS) and $n = 2$ (STAR) were selected to ensure compatibility with the viscous hydrodynamical calculations discussed below. An explicit selection on q_n was not used for these measurements; instead, they were averaged over the respective q_n distributions to give $v_n(q_{n(\mathrm{Avg.})},\mathrm{cent}) \equiv v_n(\mathrm{cent})$. The systematic errors for the ALICE, CMS and STAR measurements are reported in Refs. [30], [32] and [33] respectively.

Monte Carlo versions were used for (a) the Glauber (MC-Glauber) [34] and (b) Kharzeev-Levin-Nardi [21, 35, 36] (MC-KLN) models for fluctuating initial conditions. Each was used to compute the number of participants $\mathrm{N}_{\mathrm{part}}(\mathrm{cent})$, $q_n(\mathrm{cent})$, $\varepsilon_n(\mathrm{cent})$ [with weight $\omega(\mathbf{r}_\perp) = \mathbf{r}_\perp{}^n$] and $\bar{R}_n(\mathrm{cent})$ from the two-dimensional profile of the density of sources in the transverse plane $\rho_s(\mathbf{r}_\perp)$ [23], where $1/\bar{R}_2 = \sqrt{(1/\sigma_x^2 + 1/\sigma_y^2)}$, with σ_x and σ_y the respective root-mean-square widths of the density distributions. Computations for these initial-state geometric quantities were also made for 5% and 10% increments in q_n, from the lowest ($q_{n(\mathrm{Lo})}$) to the highest ($q_{n(\mathrm{Hi})}$) values of the q_n distribution. The computations were performed for both Au+Au ($\sqrt{s_{NN}} = 0.2$ TeV) and Pb+Pb ($\sqrt{s_{NN}} = 2.76$ TeV) collisions. From variations of the MC-Glauber and MC-KLN model parameters, a systematic uncertainty of 2-3% was obtained for $\bar{R}$ and ε (respectively) .

Figure 1(a) shows a representative q_2 distribution for

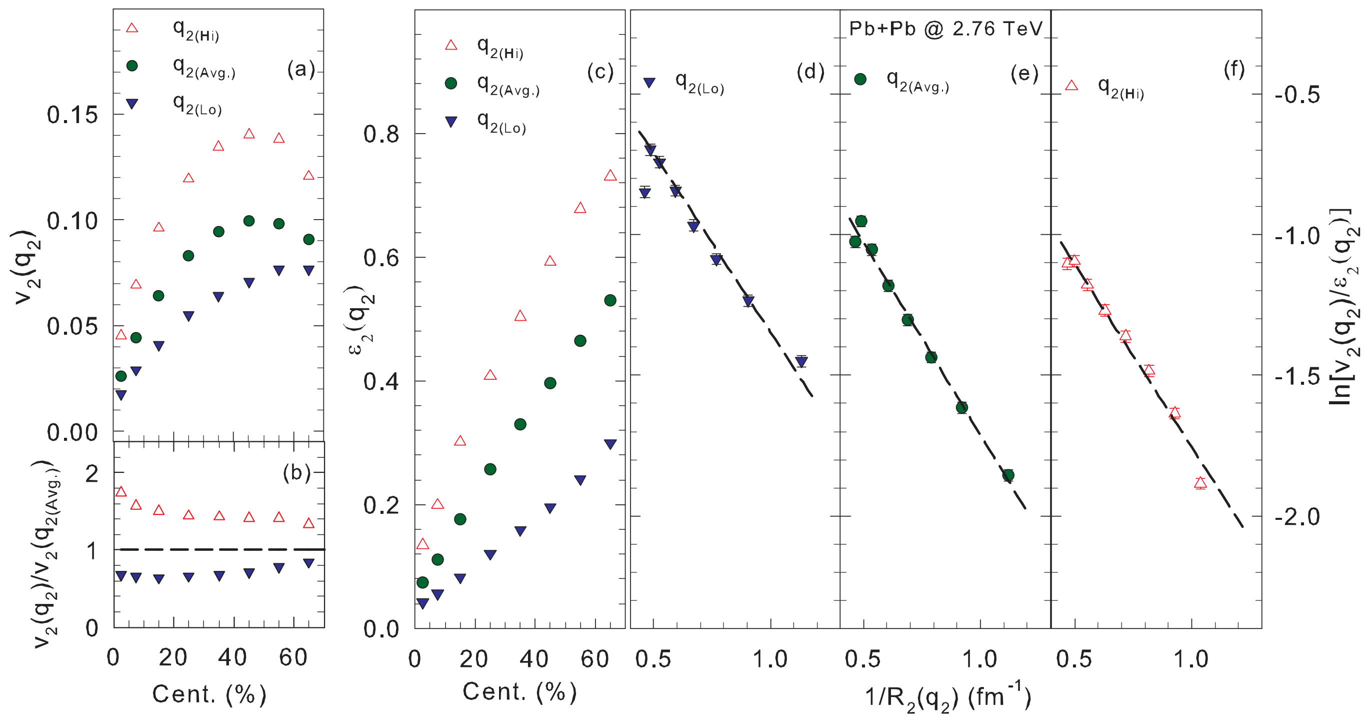

FIG. 2. (a) (Color online) Centrality dependence of $v_2(q_{2(\mathrm{Lo})})$, $v_2(q_{2(\mathrm{Avg.})})$ and $v_2(q_{2(\mathrm{Hi})})$ [30] for $0 <$ cent $< 70\%$ for Pb+Pb collisions at $\sqrt{s_{\mathrm{NN}}} = 2.76$ TeV. (b) Centrality dependence of the ratios $v_2(q_{2(\mathrm{Lo})})/v_2(q_{2(\mathrm{Avg.})})$ and $v_2(q_{2(\mathrm{Hi})})/v_2(q_{2(\mathrm{Avg.})})$. (c) Centrality dependence of $\varepsilon_2(q_{2(\mathrm{Lo})})$, $\varepsilon_2(q_{2(\mathrm{Avg.})})$ and $\varepsilon_2(q_{2(\mathrm{Hi})})$, evaluated with the MC-Glauber model. (d) $\ln[v_2(q_2)/\varepsilon_2(q_2)]$ vs. $1/\bar{R}_2(q_2)$ for $q_{2(\mathrm{Lo})}$. (e) same as (d) but for $q_{2(\mathrm{Avg.})}$. (f) same as (d) but for $q_{2(\mathrm{Hi})}$.

20-25% central MC-Glauber events for Pb+Pb collisions. The relatively broad distribution reflects the effects of sizable event-by-event fluctuations convoluted with statistical fluctuations due to finite particle number. Qualitatively similar distributions were obtained for other centralities and for other harmonics. These q_n distributions were partitioned into the 5% and 10% increments q_{nf} [from the lowest to the highest values] and used for further detailed selections on the event shape.

The effectiveness of such selections is illustrated in Fig. 1(b), which shows a strong correlation between ε_2 and q_2 for 20-25% central Pb+Pb events. Similar trends were obtained for other centrality cuts and for other harmonics. Figs. 1(c) and (d) show the dependence of ε_2 and ε_3 on $q_{2\mathrm{f}}$ for two centrality selections as indicated. For central collisions (0-5%), $\varepsilon_2(q_{2\mathrm{f}})$ and $\varepsilon_3(q_{2\mathrm{f}})$ both show an increase with $q_{2\mathrm{f}}$, albeit with a much stronger dependence for $\varepsilon_2(q_{2\mathrm{f}})$. This increase is expected to lead to a corresponding increase of $v_2(q_{2\mathrm{f}})$ and $v_3(q_{2\mathrm{f}})$ with $q_{2\mathrm{f}}$.

Fig. 1(d) indicates a similar increase of $\varepsilon_2(q_{2\mathrm{f}})$ with $q_{2\mathrm{f}}$ for 20-25% central collisions. However, $\varepsilon_3(q_{2\mathrm{f}})$ indicates a decrease with $q_{2\mathrm{f}}$, suggesting that a characteristic inversion of the dependence of $v_3(q_2)$ is to be expected as a signature in future $v_3(q_2)$ measurements for central and mid-central collisions.

Figure 2(a) shows the centrality dependence for one set of the shape-engineered measurements of $v_2(q_{2(\mathrm{Lo})}, \mathrm{cent})$, $v_2(q_{2(\mathrm{Avg.})}, \mathrm{cent})$ and $v_2(q_{2(\mathrm{Hi})}, \mathrm{cent})$ reported in Ref. [30]. They show that this event-shape selection leads to lower (higher) values of $v_2(q_2, \mathrm{cent})$ for q_2 values lower (higher) than $q_{2(\mathrm{Avg.})}$. They also show that such selections can lead to a sizable difference (more than a factor of two) between $v_2(q_{2(\mathrm{Hi})}, \mathrm{cent})$ and $v_2(q_{2(\mathrm{Lo})}, \mathrm{cent})$, as illustrated in Fig. 2(b). Strikingly similar differences can be observed in Fig. 2(c) for the MC-Glauber results shown for $\varepsilon_2(q_{2(\mathrm{Lo})}, \mathrm{cent})$, $\varepsilon_2(q_{2(\mathrm{Avg.})}, \mathrm{cent})$ and $\varepsilon_2(q_{2(\mathrm{Hi})}, \mathrm{cent})$. They suggest that differences in the measured magnitudes for $v_2(q_{2(\mathrm{Lo})}, \mathrm{cent})$, $v_2(q_{2(\mathrm{Avg.})}, \mathrm{cent})$ and $v_2(q_{2(\mathrm{Hi})}, \mathrm{cent})$, are driven by the corresponding differences in the calculated magnitudes for $\varepsilon_2(q_{2(\mathrm{Lo})}, \mathrm{cent})$, $\varepsilon_2(q_{2(\mathrm{Avg.})}, \mathrm{cent})$ and $\varepsilon_2(q_{2(\mathrm{Hi})}, \mathrm{cent})$.

The shape-selected measurements in Fig. 2(a) for $v_2(q_{2(\mathrm{Lo})}, \mathrm{cent})$, $v_2(q_{2(\mathrm{Avg.})}, \mathrm{cent})$ and $v_2(q_{2(\mathrm{Hi})}, \mathrm{cent})$ all show an increase from central to mid-central collisions, as would be expected from an increase in $\varepsilon_2(q_{2(\mathrm{Lo})}, \mathrm{cent})$, $\varepsilon_2(q_{2(\mathrm{Avg.})}, \mathrm{cent})$ and $\varepsilon_2(q_{2(\mathrm{Hi})}, \mathrm{cent})$ over the same centrality range [cf. Fig. 2(c)]. For cent $\gtrsim$ 45% however, the decreasing trends for $v_2(q_{2(\mathrm{Lo})}, \mathrm{cent})$, $v_2(q_{2(\mathrm{Avg.})}, \mathrm{cent})$ and $v_2(q_{2(\mathrm{Hi})}, \mathrm{cent})$ contrasts with the increasing trends for $\varepsilon_2(q_{2(\mathrm{Lo})}, \mathrm{cent})$, $\varepsilon_2(q_{2(\mathrm{Avg.})}, \mathrm{cent})$ and $\varepsilon_2(q_{2(\mathrm{Hi})}, \mathrm{cent})$, suggesting that the viscous effects due to the smaller systems produced in peripheral collisions, serve to suppress $v_2(q_{2(\mathrm{Lo})}, \mathrm{cent})$, $v_2(q_{2(\mathrm{Avg.})}, \mathrm{cent})$ and $v_2(q_{2(\mathrm{Hi})}, \mathrm{cent})$. This is confirmed by the symbols

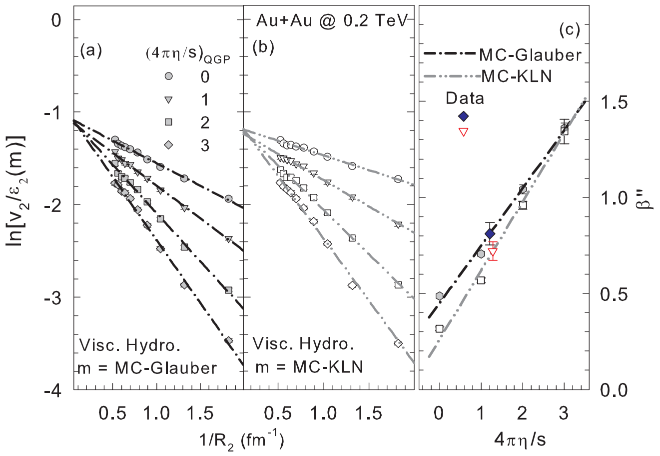

FIG. 3. (Color online) $\ln[v_2/\varepsilon_2]$ vs. $1/\bar{R}_2$ for viscous hydrodynamical calculations [31] for Au+Au collisions at $\sqrt{s_{\rm NN}} = 0.2$ TeV with (a) MC-Glauber initial-state geometries and (b) MC-KLN initial-state geometries; the dashed-dot and the dotted-dashed curves represent linear fits. Results are shown for several values of $4\pi\eta/s$ as indicated. (c) Calibration curve for β'' vs. $4\pi\eta/s$; the β'' values are obtained from the slopes of the curves shown in (a) and (b). The indicated data points are obtained from a linear fit to $\ln[v_2/\varepsilon_2]$ vs. $1/\bar{R}_2$ for the STAR Au+Au data at $\sqrt{s_{\rm NN}} = 0.2$ TeV [7, 33]

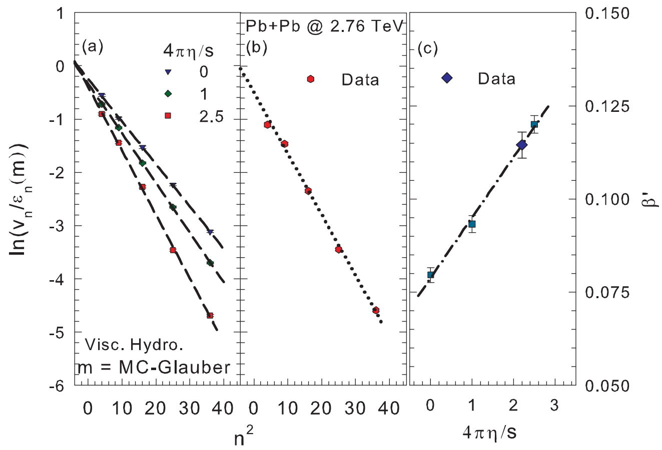

FIG. 4. (Color online) (a) $\ln(v_n/\varepsilon_n)$ vs. n^2 from viscous hydrodynamical calculations [31] for three values of specific shear viscosity as indicated. (b) $\ln(v_n/\varepsilon_n)$ vs. n^2 for Pb+Pb data. The p_T-integrated v_n results in (a) and (b) are for 0.2% central Pb+Pb collisions at $\sqrt{s_{NN}} = 2.76$ TeV [31]; the curves are linear fits. (c) Calibration curve for β' vs. $4\pi\eta/s$; the β' values are obtained from the slopes of the curves shown in (a). The indicated data point is obtained from a linear fit to the scaled data shown in (b).

and dashed curves in Figs. 2(d) - (f) which validates the expected linear dependence of $\ln[v_2(q_2)/\varepsilon_2(q_2)]$ on $1/\bar{R}_2(q_2)$ (cf. Eq. 2) for the data shown in Fig. 2(a). The dashed curves, which indicate a similar slope value ($\beta'' \sim 1.3 \pm 0.07$) for each of the scaling curves in Figs. 2(d) - (f), provide an invaluable model constraint for the event-by-event fluctuations in the initial-state density distribution, as well as for robust estimates of η/s.

The acoustic scaling patterns summarized in Eq. 2 are also exhibited in the results of q_n-averaged viscous hydrodynamical calculations [31] as demonstrated in Figs. 3(a) and (b) and Fig. 4(a). The scaled results, which are shown for several values of $4\pi\eta/s$ in each case, exhibit the expected linear dependence of $\ln(v_n/\varepsilon_n)$ on $1/\bar{R}$ for both MC-Glauber (Figs. 3(a)) and MC-KLN (Figs. 3(b)) initial conditions, as well as the expected linear dependence of $\ln(v_n/\varepsilon_n)$ on n^2 (Fig. 4(a)). They also give a clear indication that the slopes of these curves are sensitive to the magnitude of $4\pi\eta/s$. Therefore, we use them to calibrate β'' and β' to obtain estimates for $(4\pi\eta/s)_{\rm QGP}$ for the plasma produced in RHIC and LHC collisions.

Figure 3(c) shows the calibration curves for β'' vs. $4\pi\eta/s$, obtained from the viscous hydrodynamical calculations shown in Figs. 3(a) and (b). The filled circles and the associated dot-dashed curve, represent the slope parameters (β'') obtained from linear fits to the viscous hydrodynamical results for MC-Glauber initial conditions shown in Fig. 3(a). The open squares and the associated dot-dot-dashed curve, represent the slope parameters obtained from linear fits to the viscous hydrodynamical results for MC-KLN initial conditions shown in Fig. 3(b). The STAR v_2(cent) data for Au+Au collisions, also show the expected linear dependence of $\ln(v_2/\varepsilon_2)$ on $1/\bar{R}_2$ for ε_2 and $\bar{R}_2$ values obtained from the MC-Glauber and MC-KLN models respectively. The filled diamond and the open triangle in Fig. 3(c), represent the slopes extracted from the respective scaling plots that used MC-Glauber and MC-KLN initial conditions respectively. A comparison to the respective calibration curves in Fig. 3(c), gives the estimate $\langle 4\pi\eta/s\rangle_{\rm QGP} \sim 1.3 \pm 0.2$ for the plasma created in RHIC collisions. Here, it is noteworthy that our extraction procedure leads to an estimate which is essentially insensitive to the choice of the MC-Glauber or MC-KLN initial-state geometry.

The solid squares and the associated dashed-dot curve in Fig. 4(c), represent the calibration curve for β' vs. $4\pi\eta/s$, obtained from the linear fits (dashed curves) to the viscous hydrodynamical calculations shown in Fig. 4(a). Fig. 4(b) shows the expected linear dependence of $\ln(v_n/\epsilon_n)$ on n^2 for CMS Pb+Pb data [31] scaled with same ε_n values employed in Fig. 4(a). The slope extracted from Fig. 4(b) is indicated by the solid blue diamond shown in Fig. 4(c); a comparison with the the calibration curve gives the the estimate $\langle 4\pi\eta/s\rangle_{\rm QGP} \sim 2.2 \pm 0.2$ for the plasma created in LHC collisions. Note that a similar estimate is obtained from the scaling coefficient ($\beta'' \sim 1.3 \pm 0.07$) extracted from Fig. 2(e).

The $\langle 4\pi\eta/s\rangle_{\rm QGP}$ estimates for the plasma produced in RHIC and LHC collisions are in reasonable agreement with recent $\langle \eta/s\rangle$ estimates [11, 26, 36–39]. Further calculations will undoubtedly be required to reduce possible model-driven calibration uncertainties [39]. However, our method benefits from tests via implicit constraints on event-by-event fluctuations in the initial-state density distribution, as well as its lack of sensitivity to the initial-state models employed in our analysis.

In summary, we have presented a detailed phenomenological exploration of a new constraint for initial-state fluctuations, via scaling studies of v_2 measurements obtained for shape-engineered events. We find acoustic scaling patterns for shape-selected events (via $q_{2(\mathrm{Lo})}$, $q_{2(\mathrm{Avg.})}$ and $q_{2(\mathrm{Hi})}$). They provide robust tests for the event-by-event fluctuations in the initial-state density distribution. Our empirical methodology gives two consistent paths for estimating $(\eta/s)_{\mathrm{QGP}}$ of the QGP produced in Au+Au and Pb+Pb collisions at RHIC and the LHC. A calibration of the method with q_2-averaged viscous hydrodynamical model calculations, gives estimates for $(4\pi\eta/s)_{\mathrm{QGP}}$ of 1.3 ± 0.2 and 2.2 ± 0.2, for the plasma produced in Au+Au ($\sqrt{s_{NN}} = 0.2$ TeV) and Pb+Pb ($\sqrt{s_{NN}} = 2.76$ TeV) collisions (respectively). These values are insensitive to the initial-state geometry models employed.

Acknowledgments This research is supported by the US DOE under contract DE-FG02-87ER40331.A008.

* E-mail: Roy.Lacey@Stonybrook.edu

[1] D. Teaney, Phys.Rev. **C68**, 034913 (2003), arXiv:nucl-th/0301099 [nucl-th].

[2] R. A. Lacey and A. Taranenko, PoS **CFRNC2006**, 021 (2006), arXiv:nucl-ex/0610029 [nucl-ex].

[3] R. A. Lacey, N. Ajitanand, J. Alexander, P. Chung, W. Holzmann, et al., Phys.Rev.Lett. **98**, 092301 (2007), arXiv:nucl-ex/0609025 [nucl-ex]; A. Adare et al. (PHENIX Collaboration), *ibid.* **98**, 172301 (2007), arXiv:nucl-ex/0611018 [nucl-ex]; H.-J. Drescher, A. Dumitru, C. Gombeaud, and J.-Y. Ollitrault, Phys.Rev. **C76**, 024905 (2007), arXiv:0704.3553 [nucl-th]; K. Dusling and D. Teaney, *ibid.* **C77**, 034905 (2008), arXiv:0710.5932 [nucl-th]; Z. Xu, C. Greiner, and H. Stocker, Phys.Rev.Lett. **101**, 082302 (2008), arXiv:0711.0961 [nucl-th]; D. Molnar and P. Huovinen, J.Phys. **G35**, 104125 (2008), arXiv:0806.1367 [nucl-th]; R. A. Lacey, A. Taranenko, and R. Wei, (2009), arXiv:0905.4368 [nucl-ex]; K. Dusling, G. D. Moore, and D. Teaney, Phys.Rev. **C81**, 034907 (2010), arXiv:0909.0754 [nucl-th]; A. Chaudhuri, J.Phys. **G37**, 075011 (2010), arXiv:0910.0979 [nucl-th]; R. A. Lacey, A. Taranenko, R. Wei, N. Ajitanand, J. Alexander, et al., Phys.Rev. **C82**, 034910 (2010), arXiv:1005.4979 [nucl-ex].

[4] P. Romatschke and U. Romatschke, Phys.Rev.Lett. **99**, 172301 (2007), arXiv:0706.1522 [nucl-th].

[5] M. Luzum and P. Romatschke, Phys.Rev. **C78**, 034915 (2008), arXiv:0804.4015 [nucl-th]; Phys.Rev.Lett. **103**, 262302 (2009), arXiv:0901.4588 [nucl-th].

[6] H. Song, S. A. Bass, U. Heinz, T. Hirano, and C. Shen, Phys.Rev.Lett. **106**, 192301 (2011), arXiv:1011.2783 [nucl-th].

[7] K. Aamodt et al. (ALICE Collaboration), Phys.Rev.Lett. **105**, 252302 (2010), arXiv:1011.3914 [nucl-ex]; M. Luzum, Phys.Rev. **C83**, 044911 (2011), arXiv:1011.5173 [nucl-th].

[8] R. A. Lacey, A. Taranenko, N. Ajitanand, and J. Alexander, Phys.Rev. **C83**, 031901 (2011), arXiv:1011.6328 [nucl-ex].

[9] P. Bozek, M. Chojnacki, W. Florkowski, and B. Tomasik, Phys.Lett. **B694**, 238 (2010), arXiv:1007.2294 [nucl-th].

[10] T. Hirano, P. Huovinen, and Y. Nara, Phys.Rev. **C83**, 021902 (2011), arXiv:1010.6222 [nucl-th].

[11] B. Schenke, S. Jeon, and C. Gale, Phys.Rev.Lett. **106**, 042301 (2011), arXiv:1009.3244 [hep-ph]; Phys.Lett. **B702**, 59 (2011), arXiv:1102.0575 [hep-ph].

[12] H. Song, S. A. Bass, and U. Heinz, Phys.Rev. **C83**, 054912 (2011), arXiv:1103.2380 [nucl-th]; C. Shen, U. Heinz, P. Huovinen, and H. Song, **C82**, 054904 (2010), arXiv:1010.1856 [nucl-th]; F. G. Gardim, F. Grassi, M. Luzum, and J.-Y. Ollitrault, Phys.Rev.Lett. **109**, 202302 (2012), arXiv:1203.2882 [nucl-th].

[13] H. Niemi, G. Denicol, P. Huovinen, E. Molnar, and D. Rischke, Phys.Rev. **C86**, 014909 (2012), arXiv:1203.2452 [nucl-th].

[14] G.-Y. Qin, H. Petersen, S. A. Bass, and B. Muller, Phys.Rev. **C82**, 064903 (2010), arXiv:1009.1847 [nucl-th].

[15] J.-Y. Ollitrault, Phys. Rev. **D46**, 229 (1992).

[16] A. Adare et al. (PHENIX), Phys. Rev. Lett. **105**, 062301 (2010), arXiv:1003.5586 [nucl-ex].

[17] R. Lacey (PHENIX Collaboration), J.Phys. **G38**, 124048 (2011), arXiv:1108.0457 [nucl-ex].

[18] A. Adare et al. (PHENIX Collaboration), Phys.Rev.Lett. **107**, 252301 (2011), arXiv:1105.3928 [nucl-ex]; K. Aamodt et al. (ALICE Collaboration), **107**, 032301 (2011), arXiv:1105.3865 [nucl-ex]; G. Aad et al. (ATLAS Collaboration), Phys.Rev. **C86**, 014907 (2012), arXiv:1203.3087 [hep-ex]; P. Sorensen (STAR Collaboration), J.Phys. **G38**, 124029 (2011), arXiv:1110.0737 [nucl-ex]; S. Sanders (CMS Collaboration), PoS **QNP2012**, 148 (2012).

[19] P. Kovtun, D. Son, and A. Starinets, Phys.Rev.Lett. **94**, 111601 (2005), arXiv:hep-th/0405231 [hep-th].

[20] T. Hirano, U. W. Heinz, D. Kharzeev, R. Lacey, and Y. Nara, Phys.Lett. **B636**, 299 (2006), arXiv:nucl-th/0511046 [nucl-th].

[21] H.-J. Drescher, A. Dumitru, A. Hayashigaki, and Y. Nara, Phys.Rev. **C74**, 044905 (2006), arXiv:nucl-th/0605012 [nucl-th]; H.-J. Drescher and Y. Nara, **C76**, 041903 (2007), arXiv:0707.0249 [nucl-th]; Z. Qiu and U. W. Heinz, **C84**, 024911 (2011), arXiv:1104.0650 [nucl-th].

[22] B. Schenke, P. Tribedy, and R. Venugopalan, Phys.Rev.Lett. **108**, 252301 (2012), arXiv:1202.6646 [nucl-th].

[23] R. A. Lacey, R. Wei, N. Ajitanand, and A. Taranenko, Phys.Rev. **C83**, 044902 (2011), arXiv:1009.5230 [nucl-ex]; R. Snellings, J.Phys. **G38**, 124013 (2011), arXiv:1106.6284 [nucl-ex].

[24] C. Shen, S. A. Bass, T. Hirano, P. Huovinen, Z. Qiu, et al., J.Phys. **G38**, 124045 (2011), arXiv:1106.6350 [nucl-th]; Z. Qiu and U. Heinz, AIP Conf.Proc. **1441**,

774 (2012), arXiv:1108.1714 [nucl-th].

[25] R. A. Lacey, Y. Gu, X. Gong, D. Reynolds, N. Ajitanand, et al., (2013), arXiv:1301.0165 [nucl-ex].

[26] R. A. Lacey, A. Taranenko, N. Ajitanand, and J. Alexander, (2011), arXiv:1105.3782 [nucl-ex].

[27] R. A. Lacey, A. Taranenko, J. Jia, D. Reynolds, N. Ajitanand, et al., (2013), arXiv:1305.3341 [nucl-ex].

[28] E. Shuryak and I. Zahed, (2013), arXiv:1301.4470 [hep-ph].

[29] J. Schukraft, A. Timmins, and S. A. Voloshin, Phys.Lett. **B719**, 394 (2013), arXiv:1208.4563 [nucl-ex].

[30] A. Dobrin (ALICE Collaboration), Nucl.Phys. **A904-905**, 455c (2013), arXiv:1211.5348 [nucl-ex].

[31] H. Song, S. A. Bass, U. Heinz, T. Hirano, and C. Shen, Phys.Rev. **C83**, 054910 (2011), arXiv:1101.4638 [nucl-th]; See Fig. 14 in CMS PAS HIN-12-011.

[32] S. Chatrchyan et al. (CMS Collaboration), Phys.Rev. **C87**, 014902 (2013), arXiv:1204.1409 [nucl-ex].

[33] J. Adams et al. (STAR Collaboration), Phys.Rev. **C72**, 014904 (2005), arXiv:nucl-ex/0409033 [nucl-ex].

[34] M. L. Miller, K. Reygers, S. J. Sanders, and P. Steinberg, Ann. Rev. Nucl. Part. Sci. **57**, 205 (2007); B. Alver et al., Phys. Rev. Lett. **98**, 242302 (2007).

[35] D. Kharzeev and M. Nardi, Phys.Lett. **B507**, 121 (2001), arXiv:nucl-th/0012025 [nucl-th].

[36] T. Lappi and R. Venugopalan, Phys. Rev. **C74**, 054905 (2006); B. Schenke, S. Jeon, and C. Gale, Phys.Rev. **C85**, 024901 (2012), arXiv:1109.6289 [hep-ph].

[37] C. Gale, S. Jeon, B. Schenke, P. Tribedy, and R. Venugopalan, (2012), arXiv:1210.5144 [hep-ph].

[38] Z. Qiu, C. Shen, and U. Heinz, Phys.Lett. **B707**, 151 (2012), arXiv:1110.3033 [nucl-th].

[39] J. E. Bernhard, J. S. Moreland, S. A. Bass, J. Liu, and U. Heinz, (2016), arXiv:1605.03954 [nucl-th].